ISTITUTO NAZIONALE DI FISICA NUCLEARE

Sezione di Milano

INFN/TC–98/36
26 Novembre 1998

F. Alessandria, G. Ambrosio:

STUDY OF THE THERMAL SHIELD OF THE ATLAS BARREL TOROID IN CASE OF A FAST DISCHARGE

PACS: 85.25.Ly

Published by ***SIS–Pubblicazioni***
Laboratori Nazionali di Frascati

INFN – Istituto Nazionale di Fisica Nucleare
Sezione di Milano

INFN/TC–98/36
26 Novembre 1998

STUDY OF THE THERMAL SHIELD OF THE ATLAS BARREL TOROID IN CASE OF A FAST DISCHARGE

F. Alessandria, G. Ambrosio
INFN–Sezione di Milano, Laboratorio LASA, Via Fratelli Cervi 201, I–20090 Segrate (Milano), Italy

Abstract

A study of the thermal shield of the ATLAS Barrel Toroid in case of a fast discharge is presented. It consists of two parts. The first is an electromagnetic study of the shield in order to find which section will have to withstand the highest magnetic forces and to evaluate them in the *"worst condition"*. In the second part a stress analysis of this section is reported and the results are scaled to evaluate the maximum stress under different conditions.

- INTRODUCTION

The Barrel Toroid (BT) [1] is part of the magnetic system of the ATLAS detector. The complete system consists of the BT, of two End-Cap Toroids (ECTs) inserted at the ends of the BT, of an inner solenoid incorporated in the Argon Calorimeter and of an iron shield located close to the inner bore of the BT. The shield is decoupling magnetically the solenoid from the BT. A sketch of the magnetic system is shown in Figure 1.

The Barrel Toroid is made up of 8 flat coils in a racetrack configuration, assembled radially around the beam axis. Each coil is contained in its own cryostat. A thermal shield made of Al alloy surrounds each coil in order to stop the heat transmission, due to radiation and conduction, from the room temperature parts to the cold mass. The shield consists of 24 sections attached to the coil casing by means of fibreglass supports. The shield and its cross section are shown in Figure 2. It can be seen that each section consists of 4 panels (2 plane and 2 bent), 5 mm thick, joined together by means of Al alloy (Al Mg1) rivets.

The shield is cooled by He gas flowing through two pipes welded to the shield, in a symmetric position in respect to the coil plane. The inlet and the outlet temperatures are 40 K and about 80 K respectively. The flow is turbulent.

In case of a fast discharge of the BT high eddy currents are induced in the thermal shield and the resulting magnetic forces have to be carefully considered in the design of the shield and its supports.

Two kinds of eddy currents are expected:

- 2 big loops with current flowing from section to section through the He pipe along the whole shield: "global eddy currents".
- 2 loops contained within each section of the shield: "local eddy currents".

The intensity of the global eddy currents can be reduced by avoiding any contact between the start and the end of the He pipe after the valve box (the straight section of the shield on the short side of the coil has been divided in two sections to avoid a short circuit). In this way the resistance of the loop can be highly increased inserting a pipe section made of stainless steel between the valve box and the shield. According to the results shown in [2] a resistance of 3 mΩ is sufficient to reduce the peak current to few hundreds ampere. This is the situation considered in this study. On the other hand the intensity of the loops contained in each section depends only on the shield material and on the shape of the section (in this study the discharge curves are supposed to be unchangeable).

In this report both types of eddy currents are considered and the second type is studied. The central sections of the shield (i.e. those not influenced by the ECTs field and by the BT end effects) have already been analysed and the results are shown in [1]. Here the end sections are studied paying special attention to the most loaded one. The report consists of two parts. In the first part it is shown the electromagnetic study. It's aim is to find the most critical section, to calculate its coupling with the BT and the ECTs, and to calculate the maximum forces. In the second part a stress analysis of this section under the maximum forces is reported.

All FE analyses have been done using the code ANSYS 5.3 research version.

ELECTROMAGNETIC STUDY

1. - THE PROBLEM

The magnetic forces acting in the end sections of the shield in case of a fast discharge depend on the toroids (BT and ECTs) both because of their field and because of the eddy currents induced by their discharge.

The shape and the position of the shield sections require a FE analysis to evaluate the local eddy currents. Moreover the coupling between the effects of the toroid discharges (for instance the current induced by the BT interacts with the field due to the ECT) excludes the possibility of a simple addition of the forces induced by the discharge of each single toroid. Because of this complexity the study has been divided in the following steps:

- research of the section where the maximum forces are induced: *"worst section"*,
- research of the instant when the maximum forces are induced,
- study of the coupling between the BT and the worst section,
- study of the coupling between the ECT and the worst section,
- evaluation of the condition giving the maximum forces: *"worst condition"*.

2. - END SECTIONS

In order to evaluate which sections are influenced by the BT ends and by the ECTs a model of the BT including the ECTs has been done. The model shown in Figure 3 represents 1/32 of all the ATLAS magnetic system: the smallest part to generate all the system by symmetry. The inner solenoid and its yoke haven't been considered because the yoke decouples the solenoid from the BT, while it's almost completely saturated by the solenoid. Infinite elements have been used on the two faces of the model where symmetry conditions are not applied. All coils have been represented in the model: 1 coil for each double pancake of the BT, 1 coil for each ECT coil. The thermal shield is not modelled in order to have a regular mesh. 2500 scalar potential elements have been used. A static analysis has been performed to see the field shape.

In Figure 4 and 5 a frontal view and a side view of the magnetic field are shown. Overlapping to Figure 4 a sketch of the thermal shield it's possible to see that all sections but the two first are sensibly affected by the ECT field. According to the nomenclature used in Figure 2 they are: S3, S4, S5 and SE.

3. - EDDY CURRENTS IN THE END SECTIONS

The eddy currents in the end sections have been studied using a different model. It has a more complex and finer mesh than the previous one being the thermal shield included in the mesh. Because of this only the end sections near the ECT have been considered (i.e. the sections nearest the toroid axis), being the other end sections less influenced by the ECT and subjected to a lower field by the BT.

The results of the previous analysis have also been used to limit the volume of this model (see volume and mesh in Figure 6). In Figure 4 it can be seen that a condition of tangential field can be used before the start of section 3. Figure 5 shows that the same condition can be used on the top surface of Figure 6 (i.e. the cylindrical surface cutting the BT coils in their middle). These approximations have two effects on the evaluation of magnetic forces: they change the flux that generate the eddy currents and the field on the shield. Both effects have been checked comparing the two models and resulted to be negligible. The real symmetry or infinite conditions have been used on the remaining sides of the model. The other main characteristics are reported in the following list:

- The thermal shield is represented with its real thickness,
- the cross section of the shield has been slightly modified in order to have all the lateral panels on the same plane (i.e. no overlapping near the riveted junctions),
- the boxes for the cold mass supports and ribs, the sliding stops and the riveted junctions aren't considered,
- 10 mm of air separate each section from the adjacent ones,
- the He pipe between two adjacent sections is modelled as a straight pipe with an increased resistivity in order to have the same resistance of the real Omega shaped pipe,
- the mesh distribution is optimised for the computation of eddy currents having the highest density near the ends of each section,
- the material considered is Aluminium 1050 with a resistivity of 3.1 10^{-9} Ωm (RRR=15, B=0, T=60K),
- The model consists of 39000 elements: 30000 vector potential elements, 7000 scalar potential elements, 1700 vector-scalar interface elements, plus some infinite elements and current source elements. The database requires about 102 MB.

The part of thermal shield included in the model is shown in Figure 7.

4. - TRANSIENT ANALYSIS

This model has been used to evaluate the magnetic forces due to eddy currents in case of a discharge of the BT. The field generated by the ECT is supposed to remain constant. Both the extreme conditions have been studied: ECT at maximum field and at zero field.

During a fast discharge of the BT an high current is induced in the casing. This current has been analytically calculated in [2]. Here it is added to the current flowing in the coils.

time	I	dI/dt
(s)	(kA)	(kA/s)
1	2457	2.58
33	2273	9.57
47	2071	19.40
60	1744	29.79
73	1335	31.83

Table 1: The total current and its derivative in the five instants when forces have been evaluated.

In order to evaluate where and when the highest forces are induced, eddy currents and magnetic forces have been computed and compared in 5 instants during the discharge. The total current in the coil (Icoil + Icasing) and its derivative used in these instants are reported in Table 1. In order to have correct results in each step of the study, a unique transient analysis from the start of the discharging to the last instant (73 s) has been done. Different time steps have been used: big steps (10 s maximum) in the middle between two studied instants, shorter and shorter steps (0.1 s minimum) when approaching a studied instant.

5. - RESEARCH OF THE *"WORST SECTION"*

An example of the results is shown in Figure 8 where the eddy currents are shown 60 s after the start of the discharge. The arrows represent the current density in A/m^2. Both their length and colour are related to the current intensity while the density of the arrows is only an effect of the mesh density. The local eddy currents can be easily recognised. The arrow exiting from the He pipe in the lower left part of the model represents the global eddy current. The highest density occurs in the ends of the sections where local and global eddy currents overlap. High currents cross the top and bottom panels of section 3 and 4 and the top panel of the curved section. For instance the current density at the top of section 3 is 10^6 A/m^2.

The magnetic forces 60 s after the start of the BT discharge, with the ECT remaining at maximum current, are shown in Figure 9. They are presented as specific forces (N/m^2: i.e. the force acting on an element over the element surface). The main characteristics are: a big force toward the centre of the coil on the upper and lower panels (for instance the maximum pressure on the top panel of section 3 is about 4 KPa), a moment around the He pipe on the side panels, a force that is trying to stretch the side panels. Section 3 is subjected to the highest loads (it's the same without the ECT field).

The eddy currents and the total magnetic force on the model of sections 3 and 4 (half section because of symmetry) are reported in Figures 10 and 11. Also the global eddy current is shown in Figure 10[1]. They have been evaluated in the studied instants with the ECT remaining at maximum current.

It can be seen that the maximum forces occur after 60 s even if the highest currents are induced after 73 s (it's the same without the ECT field). This is due to the fact that from 60 to 73 s the decreasing of the field is more relevant than the small increment of the eddy currents. After 73 s the slope of the I(t) curve decreases and the magnetic forces cannot increase anymore.

6. - COUPLING OF THE *"WORST SECTION"* WITH THE TOROIDS

The coupling between section 3 and the toroids have been studied using a third model. This is a short version of the previous one consisting of 21000 elements. In fact it contains only section 3 and 4 using an artificial boundary condition (tangential field) after section 4.

---

[1] The values of the global eddy current here reported are only indicative of its behaviour because this model is not optimised for its computation.

This condition effects the field on the end of section 4 while has a negligible influence on section 3.

This model has been used to evaluate:

- The time constant (τ) of the currents induced by the discharging of the toroids (BT and ECT).
- The coupling constant $\alpha = -M/R$, where M is the mutual inductance between a toroid and section 3 and R is the electrical resistance of the shield to the eddy current induced by the same toroid.

In case of a constant variation of the current (I_{source}) in the BT or in the ECT the intensity of the eddy current (I_{eddy}) is given by the following equation:

$$I_{eddy}(t) = \alpha \frac{dI_{source}}{dt}\left(1 - e^{-\frac{t}{\tau}}\right)$$

The couplings of section 3 with the BT and the ECT have been studied separately in the following way:

- a transient analysis is started with a constant current flowing in the toroid (to improve the numerical precision),
- a discharge of the toroid with a constant dI/dt is set for 2 s,
- the discharge continues for two more seconds with a constant value of dI/dt that is half the previous value.

An example of the results is reported in Figure 12 where the coupling with the ECT is shown. The square marks show the computed values of the eddy current. The time step used is shorter at the start of each new slope (0.1 s) and longer at the end (0.4 s). The time constant is obtained by fitting the two curves. The coupling constant (α) is given by the ratio between the asymptotes of the two curves over and the value of the discharge rate (dI/dt). The triangular marks show a check: they are the value of dI/dt times the estimated value of coupling constant (i.e. they should stay on the lines asymptotic to the eddy current curve).

In Figure 13 there are the eddy currents induced by the ECT on section 3 and 4 after 2 s with a constant discharge rate of dI/dt=80000 A/s (this is the highest value foreseen in the ECT Technical Design Report [3]). It can be noted that the current distribution on section 3 is quite different from that due to the BT. For instance the centre of the vortex is closer to the right side of the section. For a comparison with the previous case, the highest values of the current density are: $4\ 10^5$ A/m^2 on the top panel and $8\ 10^5$ A/m^2 on the bottom panel.

The results of this analysis are summarised in Table 2.

	BT	*BT*	*ECT*	*ECT*
	α	τ (s)	α	τ (s)
Section 3	0.085	0.41	0.017	0.47
Section 4	0.047	<0.4		
Global loop	0.013	<0.2	<0.001	<0.2

Table 2: Coupling of the BT and the ECT with section 3. The couplings of the BT with section 4 and the global loop are also reported for comparison.

The difference between the time constants of the currents induced on section 3 by the BT and the ECT is an effect of the difference between the current loops. The values of the

coupling constant (a) given by the BT is five times greater than that by the ECT, but this difference is partially compensated by the higher dI/dt of the ECT discharge. Some results regarding the global eddy current are also reported for comparison. Neither this model nor the previous one are optimised for this computation, but having used in the two models opposite approximations the real value of the coupling between the BT and the global loop should be between 0.013 and 0.009 (result of the previous model).

7. - RESEARCH OF THE "WORST CONDITION"

The *"worst condition"* occurs when the discharges of the BT and of the ECTs overlap their effects in order to give the highest magnetic forces. Using the previous results this condition is estimated to occur 60 s after the start of the BT discharge and 25 s after the start of the ECTs discharge. This is an approximated estimation taking into account the followings notes:

- The eddy current and the magnetic field generated by each toroid depend on the time elapsed from the start of the fast discharge of the same toroid. The two discharges are assumed to be independent: in the following -*t'*- is the time from the start of the BT discharge and -*t''*- from that of the ECTs.
- Naming $f(t',t'')$ the magnetic force density, J_{eddy_XT} the density of the eddy current generated by the X toroid and B_{XT} its magnetic field, it is:

$$\vec{f}(t',t'') = \left(\vec{J}_{eddy\_BT}(t') + \vec{J}_{eddy\_ECT}(t'')\right) \times \left(\vec{B}_{BT}(t') + \vec{B}_{ECT}(t'')\right)$$

and the problem is to found t' and t'' giving the highest value of the integral of the force density on the selected section.

- The ECT has a stronger influence because of its eddy currents than because of its magnetic field. In fact the time when the worst condition occurs in case of a fast discharge of the BT only, is not affected by the magnetic field of the ECT (i.e. in this case the worst condition occurs after about 60 s both with and without the magnetic field generated by the ECT), while the maximum current induced by the ECT on section 3 is quite near the one induced by the BT.

  Therefore the contribution of the ECT to the worst condition occurs when its discharging curve reaches the maximum slope resulting in the highest eddy current. According to the ECT TDR [3] it is at $t'' = 25$ s. Therefore the problem becomes to find the maximum of $\int_{Section3} \vec{f}(t',25) \cdot da$.

- Because of the low influence of the ECT magnetic field, the function $df(t',25)$ can be reduced to the following:

$$\vec{f}(t',25) \equiv \left(\vec{J}_{eddy\_BT}(t') + \vec{J}_{eddy\_ECT}(25)\right) \times \vec{B}_{BT}(t')$$

- Assuming the two eddy currents to have the same distribution the problem becomes the research of the maximum of the following scalar function:

$$\left|\vec{f}(t',25)\right| \propto \left(J_{eddy\_BT}(t') + J_{eddy\_ECT}(25)\right) \cdot B_{BT}(t')$$

- Taking into account the results of the study of the coupling between the toroids and section 3, and naming $I_{XT}(t)$ the current flowing in the X toroid at the time t, the function becomes:

$$\left|\vec{f}(t',25)\right| \propto \left(0.085\frac{dI_{BT}}{dt}(t') + 0.017\frac{dI_{ECT}}{dt}(25) \right) \cdot I_{BT}(t')$$

We remark that the values 0.085 and 0.017 are the ratios between the total eddy current induced on Section 3 by each toroid and its discharging rate. Assuming the eddy currents to have the same distribution on the shield, it is:

$J_{eddy\_BT}(x,t') = c(x)\, I_{eddy\_BT}(t')$ and $J_{eddy\_ECT}(x,t'') = c(x)\, I_{eddy\_ECT}(t'')$ where $c(x)$ is the same for BT and ECT.

Inserting the data of the discharging curves this problem can be easily solved. In this study the discharging curves have been taken from [2,3]. The result is that the worst condition occurs in case the ECT discharge starts 35 s after the start of the BT discharge. The characteristics of the worst condition are reported in Table 3.

		BT	*ECT*
Time from the start of each fast discharge	S	60	25
Current	KA	1800	1580
dI/dt	KA/s	30	80
Eddy current induced in section 3	A	2550	1360
Global eddy current	A	400	<70

Table 3: Characteristics of the *"worst condition"*.

8. - MAGNETIC FORCES IN THE "WORST CONDITION"

Taking into account the previous results the magnetic forces acting on section 3 in the "worst condition" have been evaluate using the last model under the following conditions:

- A transient analysis is performed for two seconds with a constant discharge rate (dI/dt) in both the toroids.
- The discharge rates are those occurring in the "worst condition" (see Table 3).
- The starting value of both currents is computed in order to have after two seconds the currents occurring in the "worst condition" (see Table 3).
- 10 substeps are used in the transient analysis in order to have the best accuracy.

The resulting eddy current density and the specific forces are plotted in Figures 14 and 15 the total force is reported in Table 4.

All models used up to now haven't the aperture in the shield for the cold mass supports. The value of this approximation depends on how the support shield will be joined to the rest of the thermal shield. The previous analyses (see for instance Figure 8) have shown that much eddy current crosses this region. This fact suggests to design the junction with the support

shield in order to avoid the creation of an electrical bridge (for instance setting the thermal contact on one side only). In order to study the effect of such a solution a new model have been done with an hole in the position of the aperture. Also the mesh density has been augmented in respect to the previous model to increase the accuracy. The results are show in Figures 16, 17 and Table 4

		1st model	2nd model
Fx	N	-4211	-3501
Fy	N	9092	8770
Fz	N	-306	-285

Table 4: Total force on half section 3 in the worst condition evaluated using two models: with and without an hole in the position of the aperture for the cold mass support.

STRESS ANALYSIS

1. - TWO MODELS

The magnetic forces computed in the worst condition in section 3 have been used as load in a stress analysis of the same section. Two models have been used. They have the same characteristics of the electromagnetic models presented in the last section (i.e. with and without the aperture for the cold mass supports). The models are made of 560 and 900 linear "shell" elements 5 mm thick. The elements are set in the same position of the outer surface of the shield used in the electromagnetic study. The same mesh of the electromagnetic model is used in order to allow an automatic transfer of the forces to the structural models. The forces are multiplied by a factor two because only the forces on the nodes of the outer surface of the electromagnetic model are transferred. The error of this approximation is about 1 %.

The main approximations used for both models are:

- The riveted junctions are not considered.
- The apertures for the coil ribs are neglected.
- No temperature dependence of the Young modulus (69 GPa) is considered.

In the first model 12 supports (six on each lateral panel) are supposed to constrain the section to the coil casing. They are modelled as displacement and rotation constraints applied on some nodes of the shield. In figures 18 they are shown together with the constraints due to symmetry conditions:

A) The "fix point" with constraints in all directions and rotations.
B) A support allowing displacements in the direction of the Y-axis only (in order to accommodate the different thermal contractions of the shield and the coil casing).
C) Two supports allowing displacements in the Z direction only.
D) Two supports constraining only displacements in the direction normal to the shield (X-axis).

Seventeen supports are used in the second model. Their modelling depend on the characteristics of the final drawings of the supports:

E) The "fix point" with constraints in all directions.
F) Five supports on each lateral panel constraining only displacements in the direction normal to the shield (X-axis).
G) Five supports on the symmetry plane of the shield constraining only displacements toward the centre of the coil (i.e. Y direction).

2. - FIRST MODEL

The results of this analysis are shown in Figures 19 and 20. The greatest displacement occurs at the top of the shield (3.2 mm) and there is also a sensible tendency to the shrinking of the lateral panel (about 2.4 mm). The equivalent stresses (Von Mises) are shown in Figure 20. The highest value is caused by the method adopted to model the supports. A better evaluation of the maximum stress is to choose the highest value among all the nodes where no constraints are applied. In this way the maximum equivalent stress results 30 MPa.

3. - SECOND MODEL

The displacements resulting from the stress analysis of this model are shown in Figure 22. The maximum displacement is 2.2 mm and is due to the shrinking of the lateral. The maximum significant stress (evaluated as in the previous case) is again 30 MPa.

Comparing the results of the two models the supports used in the second one result to be less efficient (giving the same stress under lower forces). This is due to decision of using supports simpler and easier to be assembled than those foreseen for the first model.

4. - SCALING OF THE RESULTS AND CONCLUSIONS

According to these results a maximum equivalent stress of about 30 MPa is to be expected if using an Aluminium alloy with an electrical resistivity of $3.1\ 10^{-9}\ \Omega m$. This is the resistivity of a material having RRR=15 at the temperature of 60 K. As it is shown in the Technical Design Report [1] some sections of the shield will have a temperature of about 40 K. Moreover if the alloy 1050 will be used its RRR value cannot be requested in the specifications and a conservative value of 50 (for the eddy current problem) must be taken into account in the mechanical design.

Being both the magnetic and the stress analysis here shown linear analyses the results can be easily scaled to evaluate the maximum stress under different conditions. In Table 5 it's shown the maximum stress foreseen at the temperatures of 60 and 40 K and for an alloy with RRR equal to 15 or 50.

T / RRR	60 K	40 K
15	30 MPa	44 MPa
50	58 MPa	116 MPa

Table 5: Equivalent stress under different conditions (RRR and temperature). It is reported the maximum value in a node without constraints.

It should be noted that these values are the results of a research involving three different analyses: the study of the discharge curves, the research and evaluation of the maximum magnetic forces and the stress analyses. The first and the second step of this path are quite complex and their uncertainty is difficult to be evaluated. This is even more true for the final results.

An adequate safety margin, taking into account also this uncertainty, is to be adopted in the design of the shield. The 0.2% PS stress at room temperature of the Al alloy 1050 (state 0) is 25 MPa. We therefore suggest the use of a different Al alloy with an higher electrical resistivity and better mechanical properties than 1050.

REFERENCES

[1] *"ATLAS Barrel Toroid Technical Design Report"*
ATLAS TDR 7, CERN/LHCC/97-19 (1997).

[2] E. Acerbi, M. Sorbi
"Eddy currents calculation in the thermal shield of the Barrel Toroid and B0 coils: approach by means of coupled circuits",
LASA/ATLAS/13.

[3] *"ATLAS End Cap Toroids Technical Design Report"*
ATLAS TDR 8, CERN/LHCC/97-20 (1997).

List of figures:

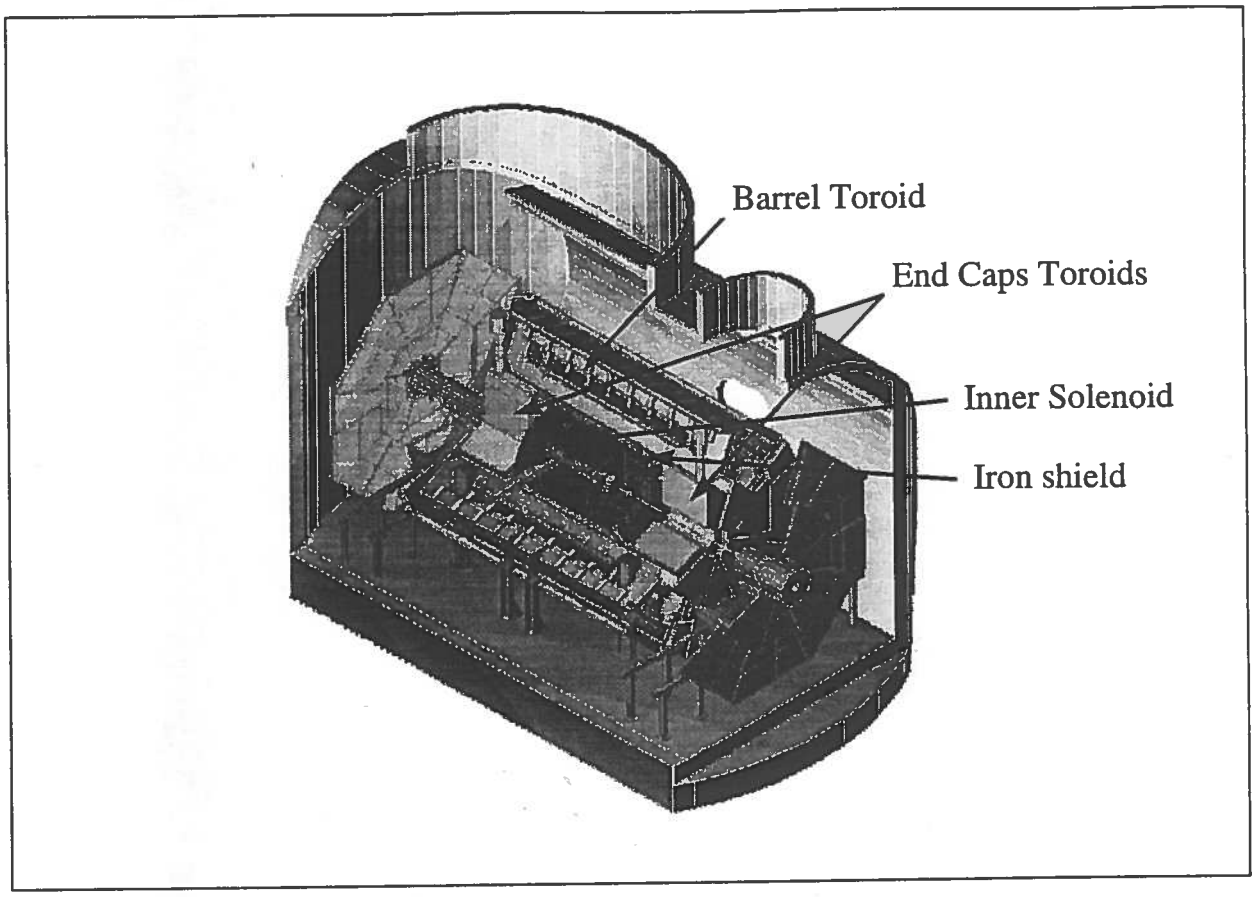

Figure 1: ATLAS magnetic system.

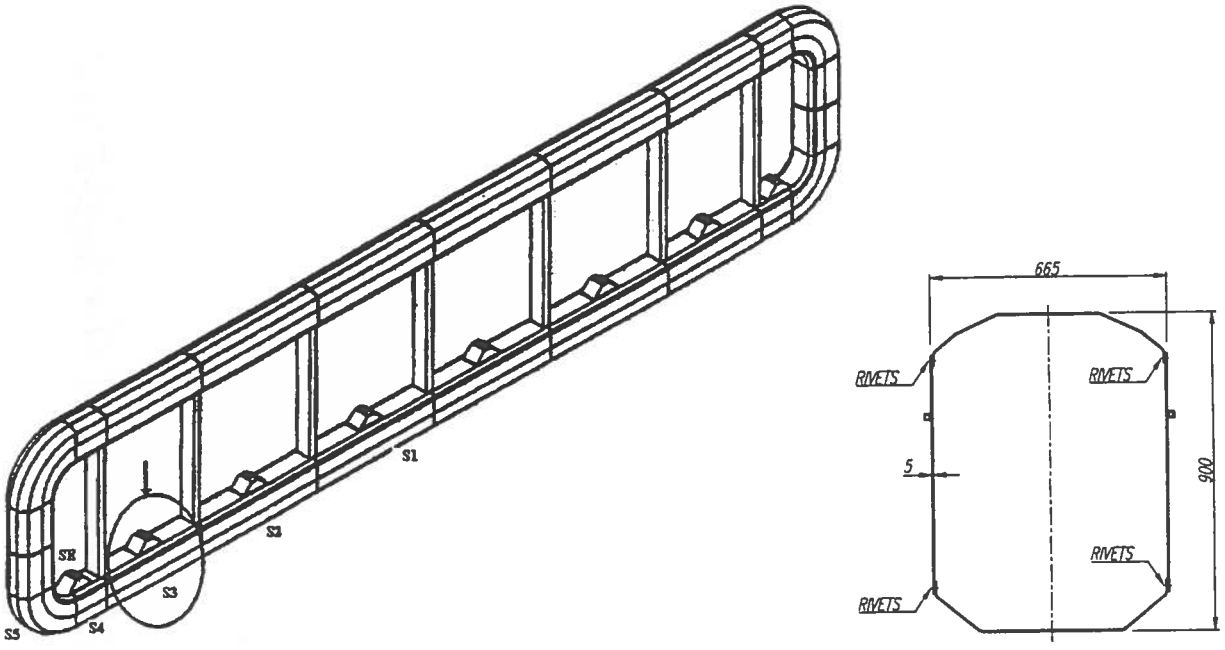

Figure 2: The thermal shield of a coil and its cross section.

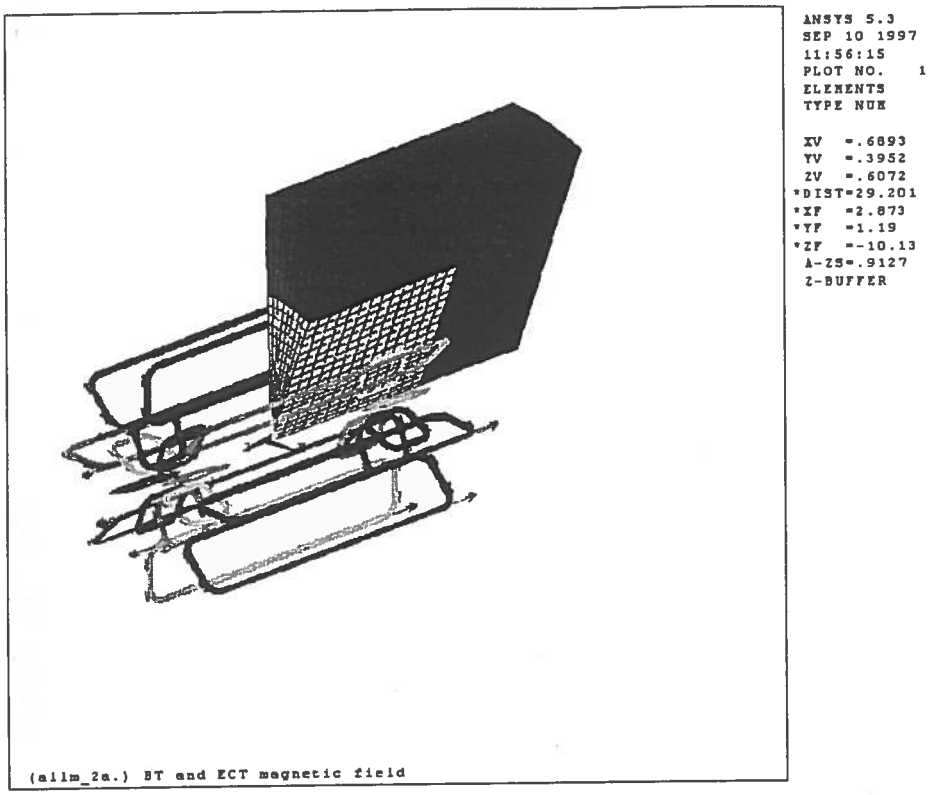

Figure 3: Model used to study the magnetic field on the whole thermal shield.

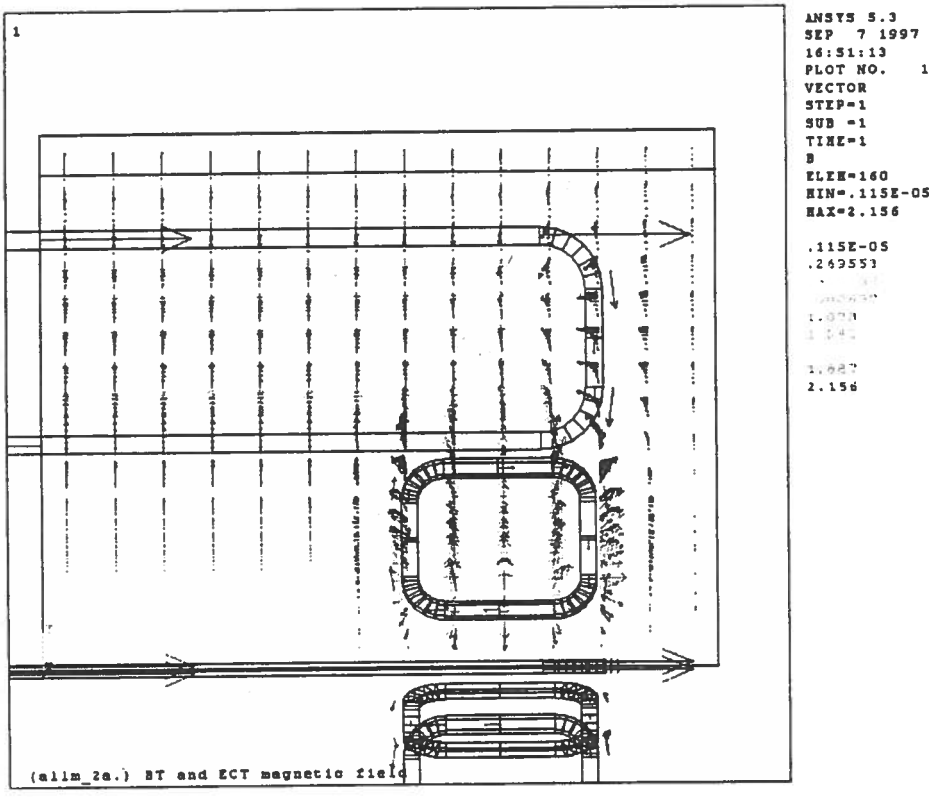

Figure 4: Frontal view of the magnetic field.

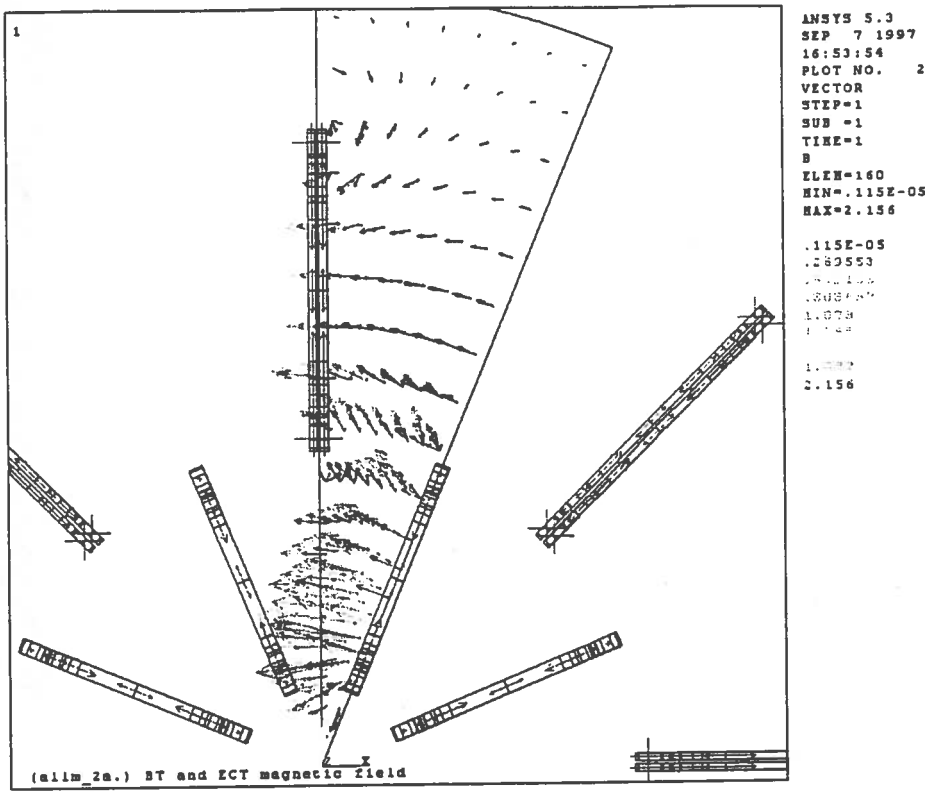

Figure 5: Side view of the magnetic field.

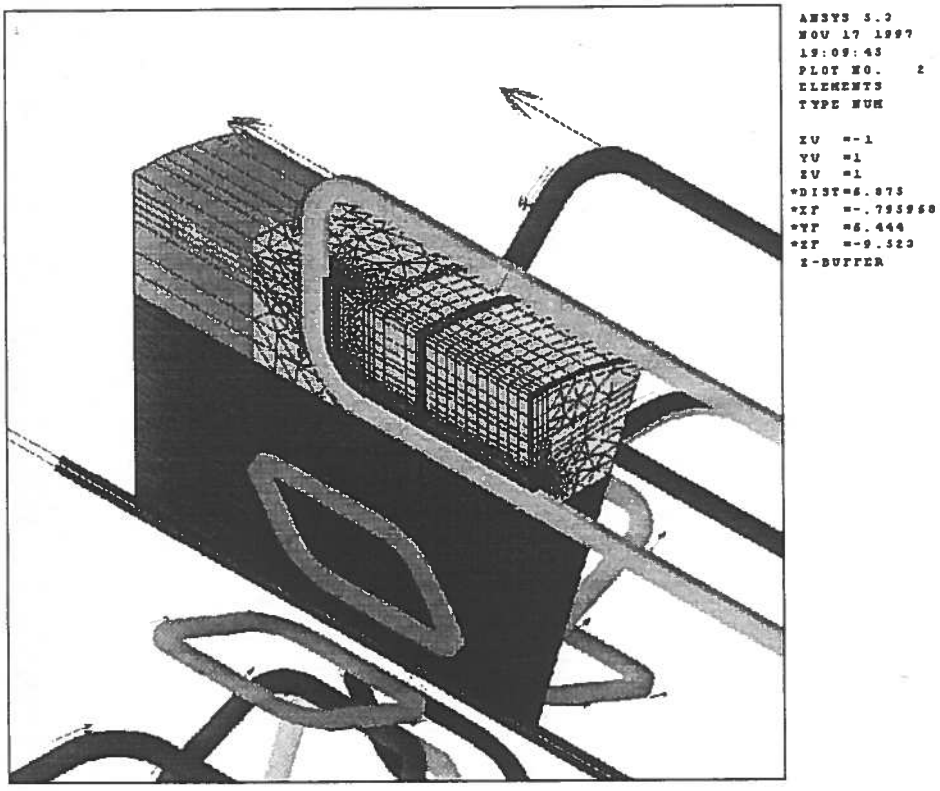

Figure 6: Model used for the study of the eddy currents in the end sections.

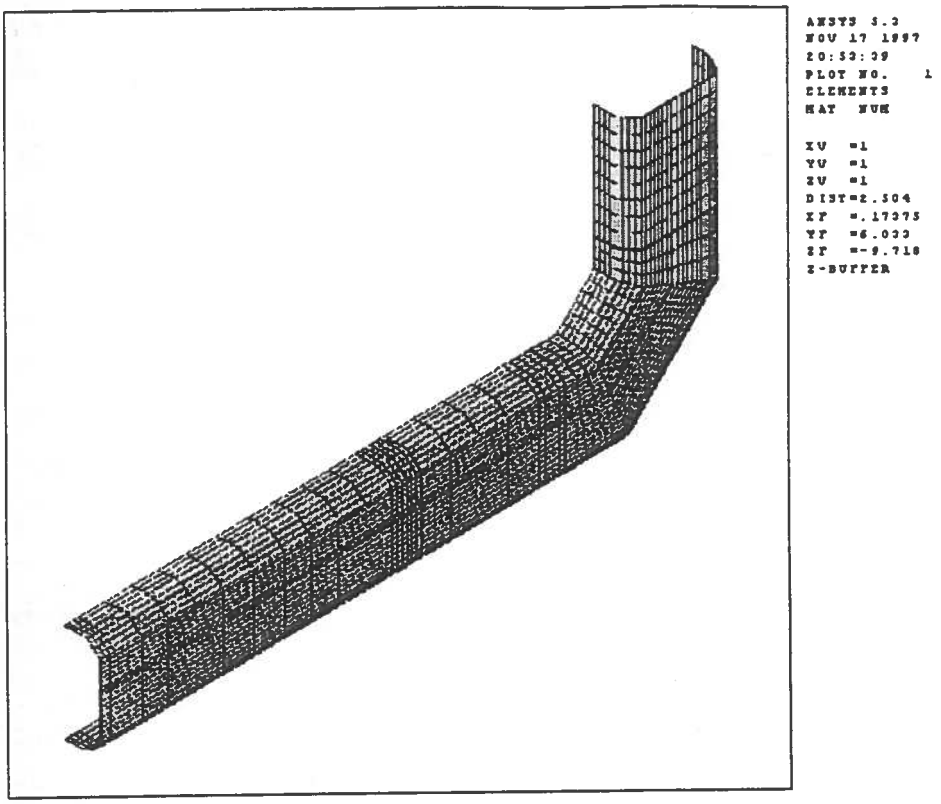

Figure 7: The model of the thermal shield.

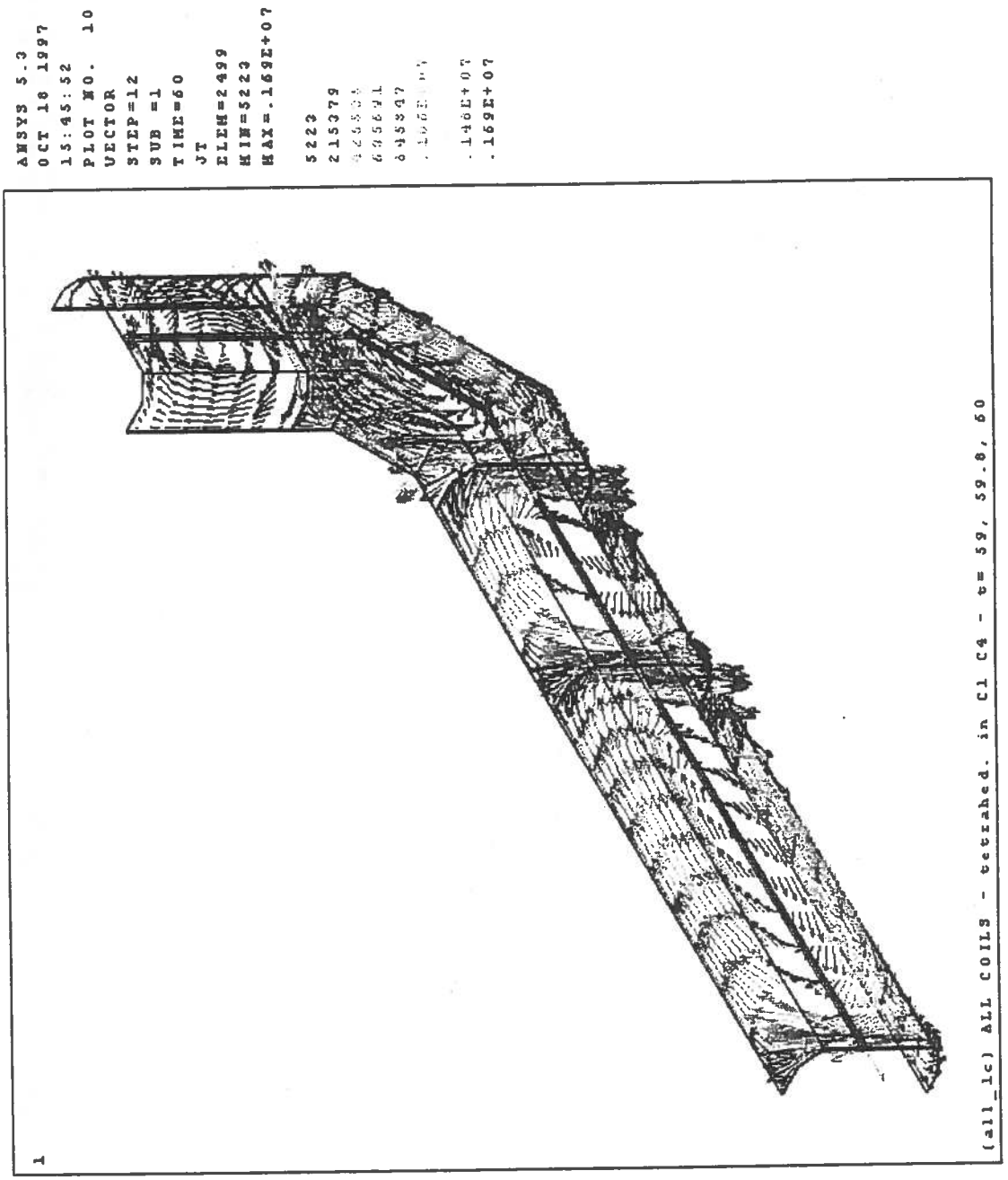

Figure 8: Eddy currents after 60 s.

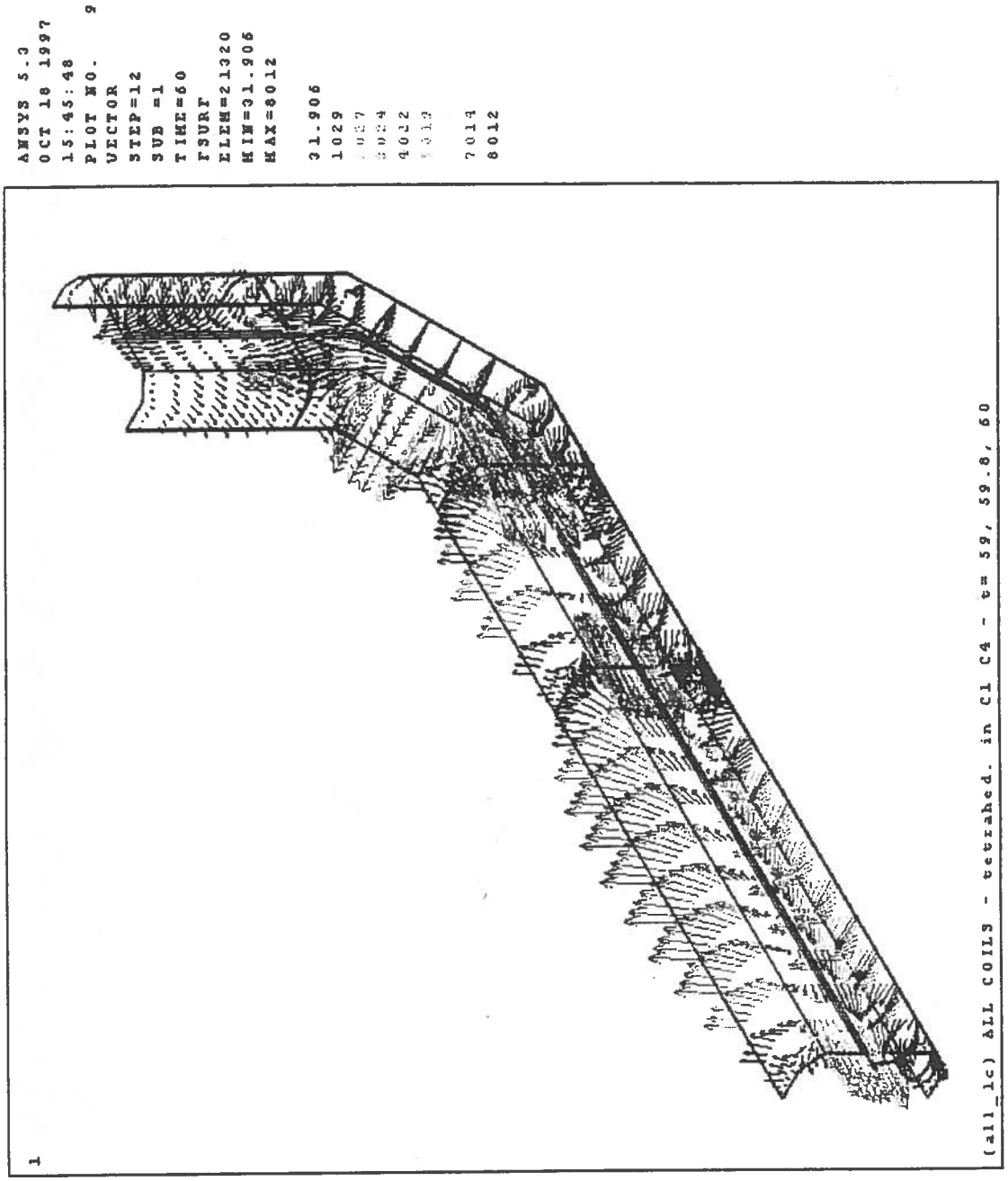

Figure 9: Magnetic forces after 60 s with the ECT at maximum current.

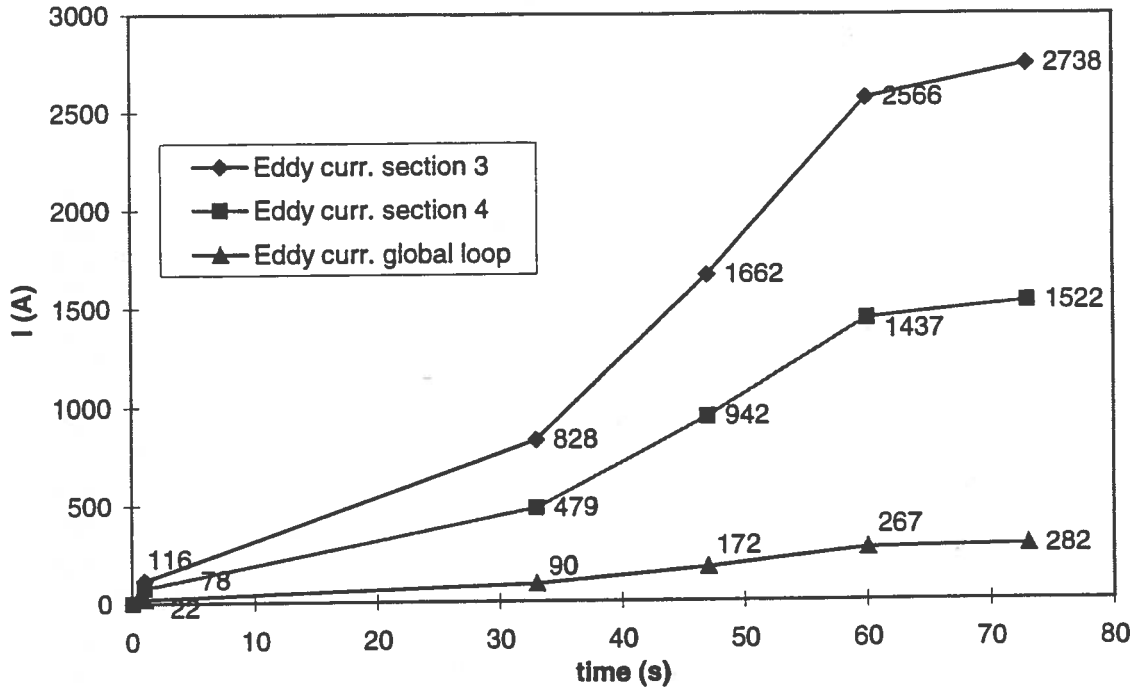

Figure 10: Eddy currents induced by a fast discharge of the BT in section 3, 4 and in the global loop.

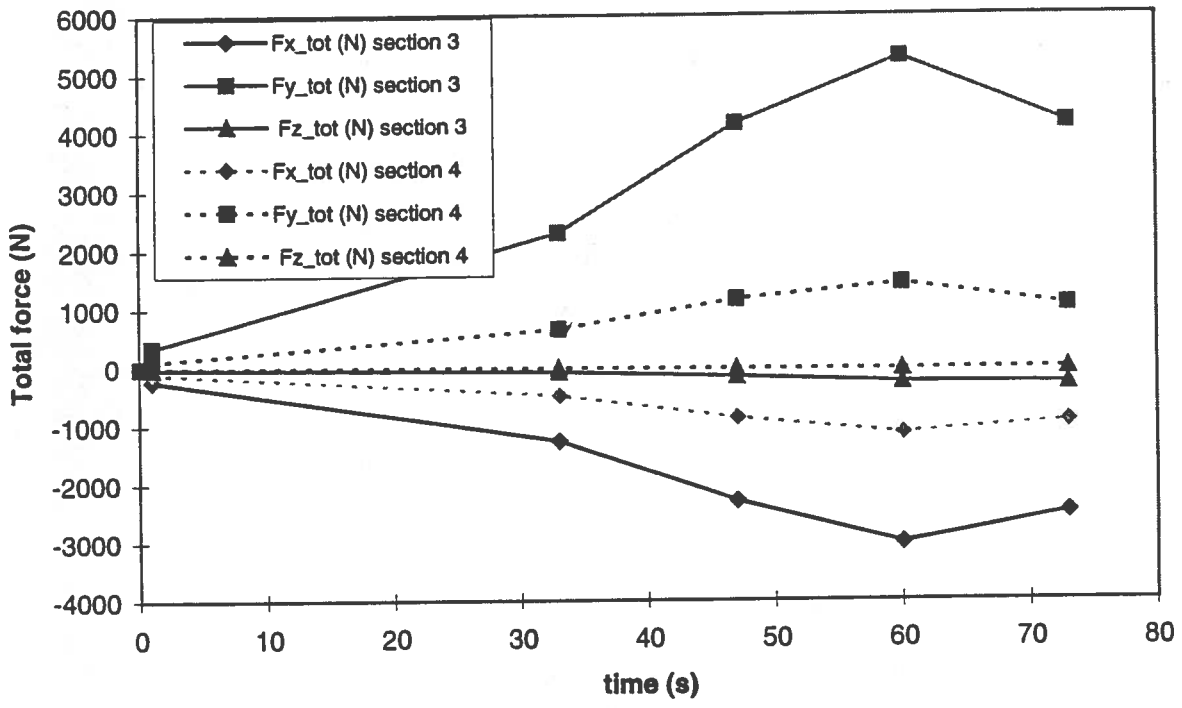

Figure 11: Total force on section 3 and 4 in case of a fast discharge of the BT while the ECTs remain at maximum current.

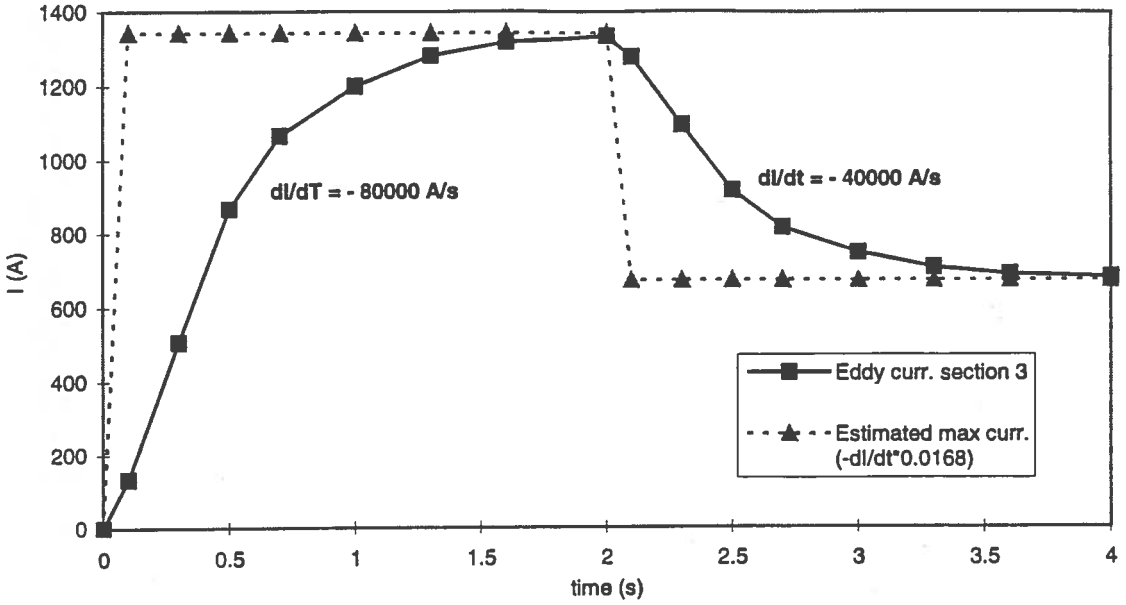

Figure 12: Study of the coupling between section 3 and the ECT.

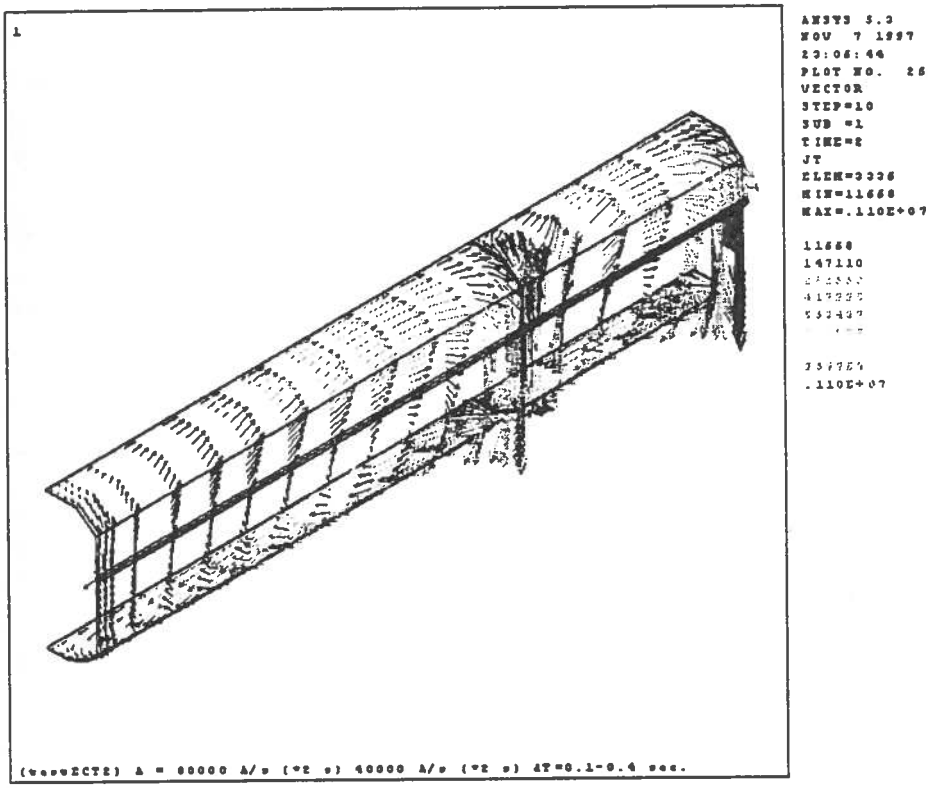

Figure 13: Eddy currents induced by the ECT discharge.

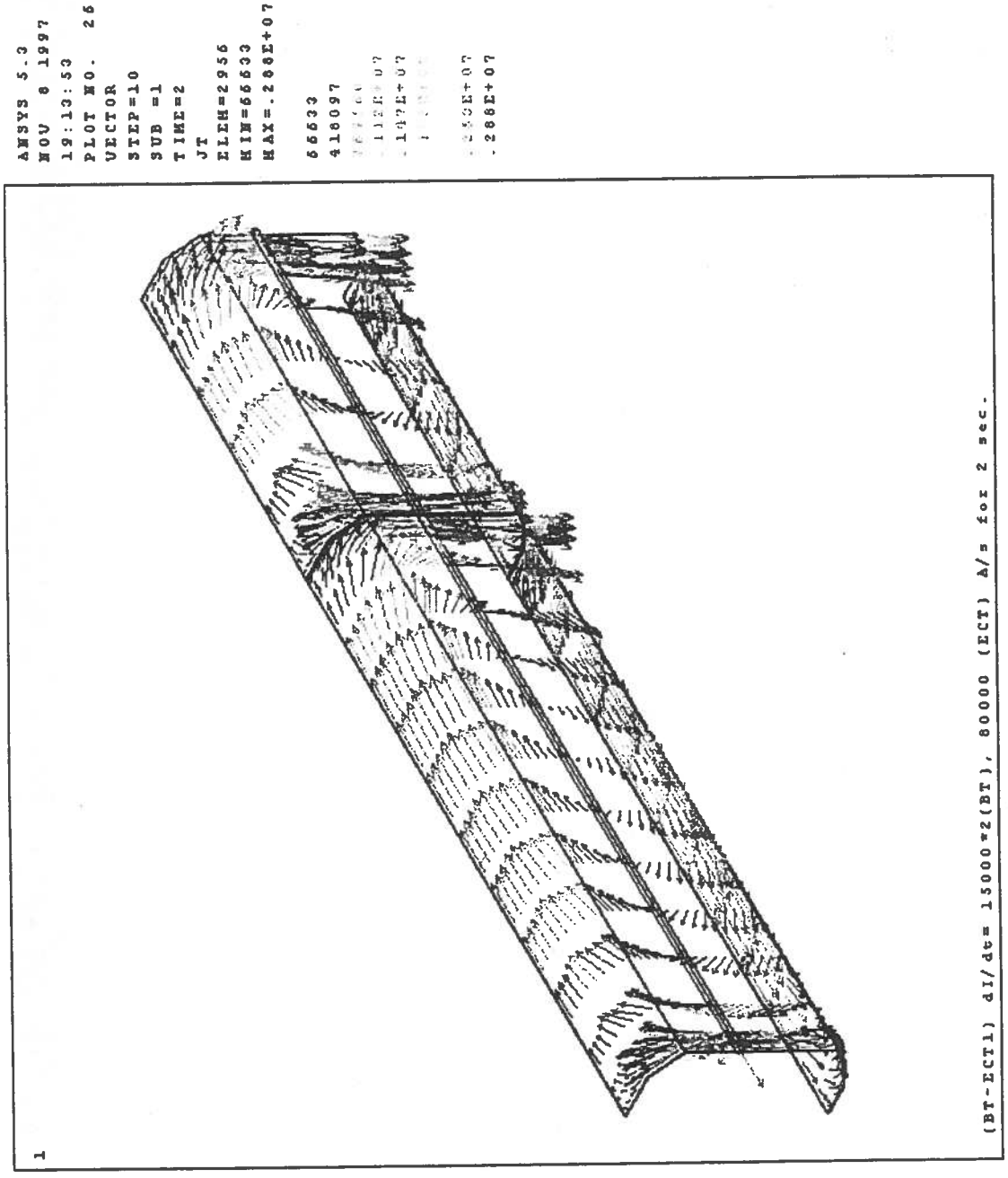

Figure 14: Eddy currents in the *worst condition*.

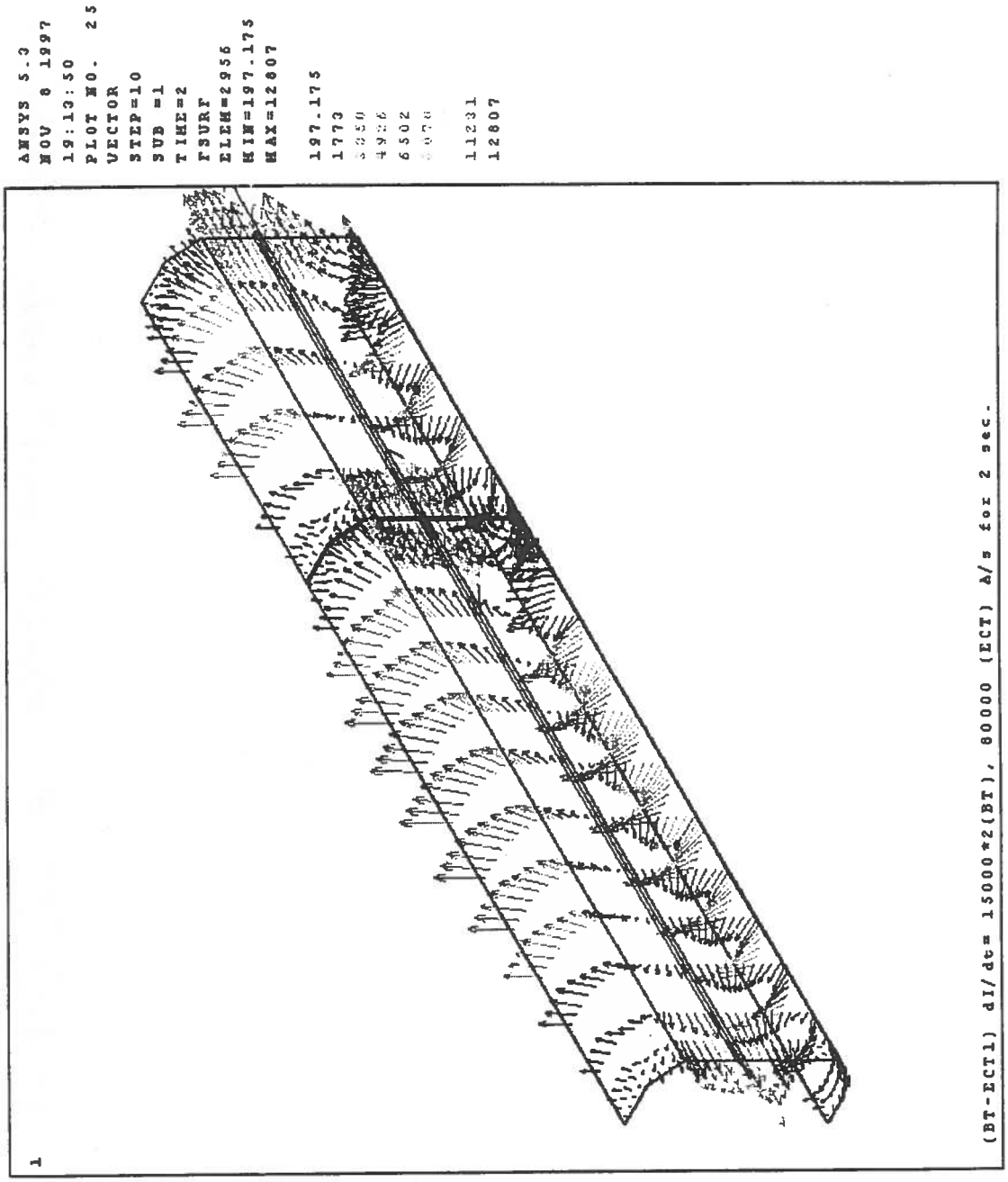

Figure 15: Specific forces in the *worst condition*.

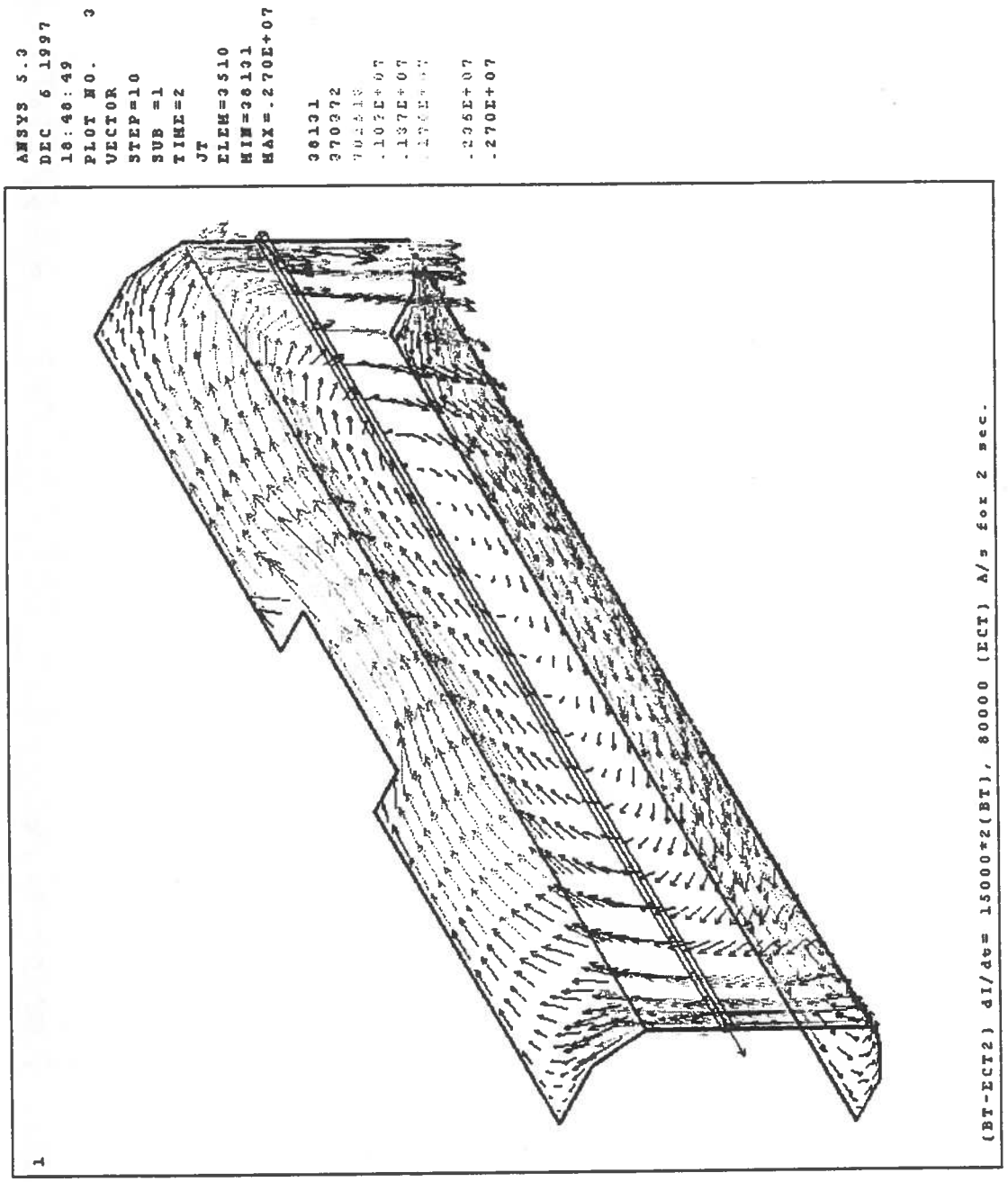

Figure 16: Eddy currents in the *worst condition* evaluated using a model of the shield with an hole in the position of the aperture for the cold mass support.

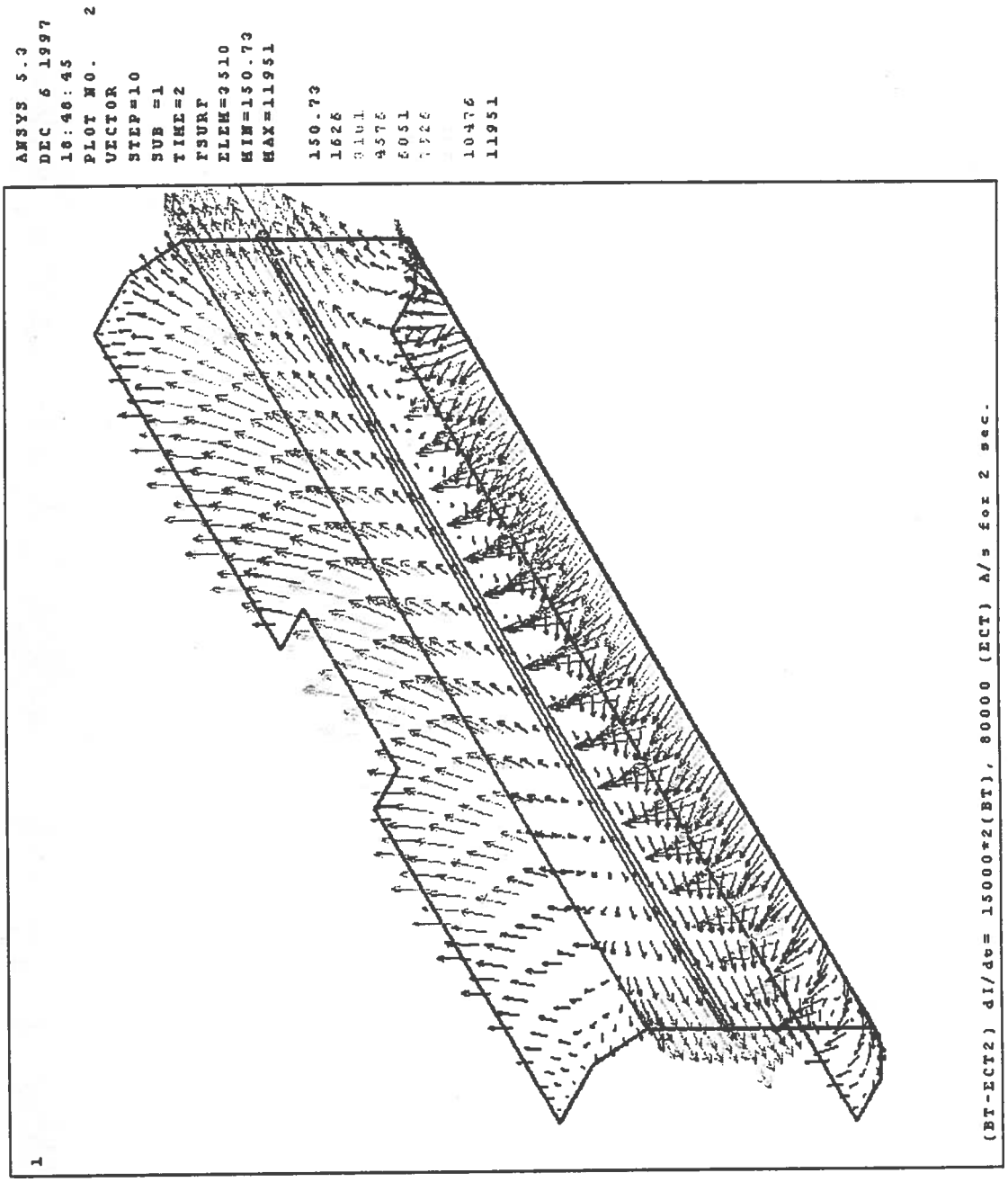

Figure 17: Specific forces in the *worst condition* evaluated using a model of the shield with an hole in the position of the aperture for the cold mass support.

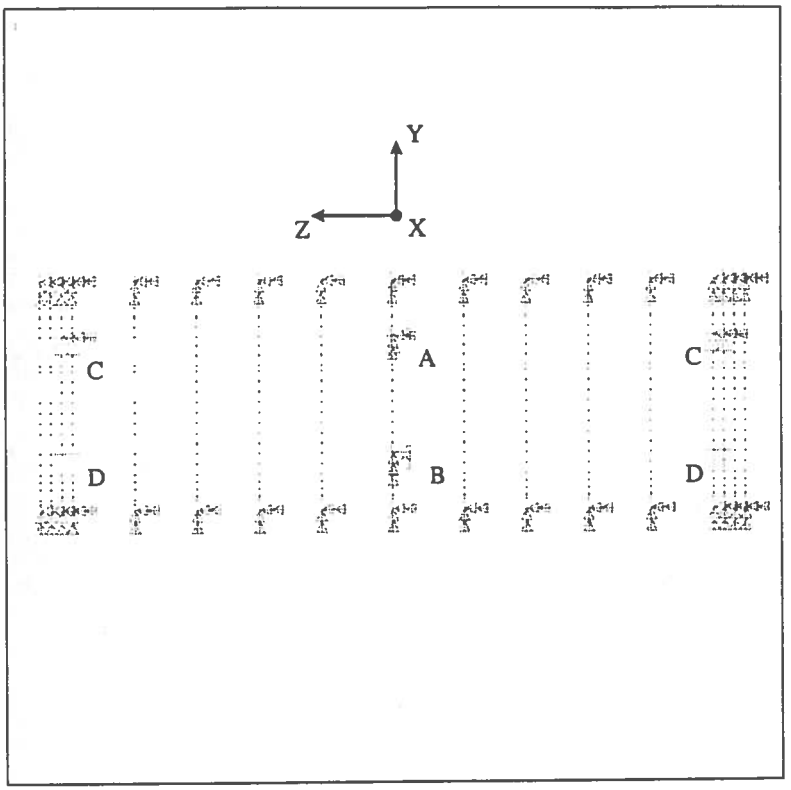

Figure 18: Constraints for stress analysis - model without the aperture.

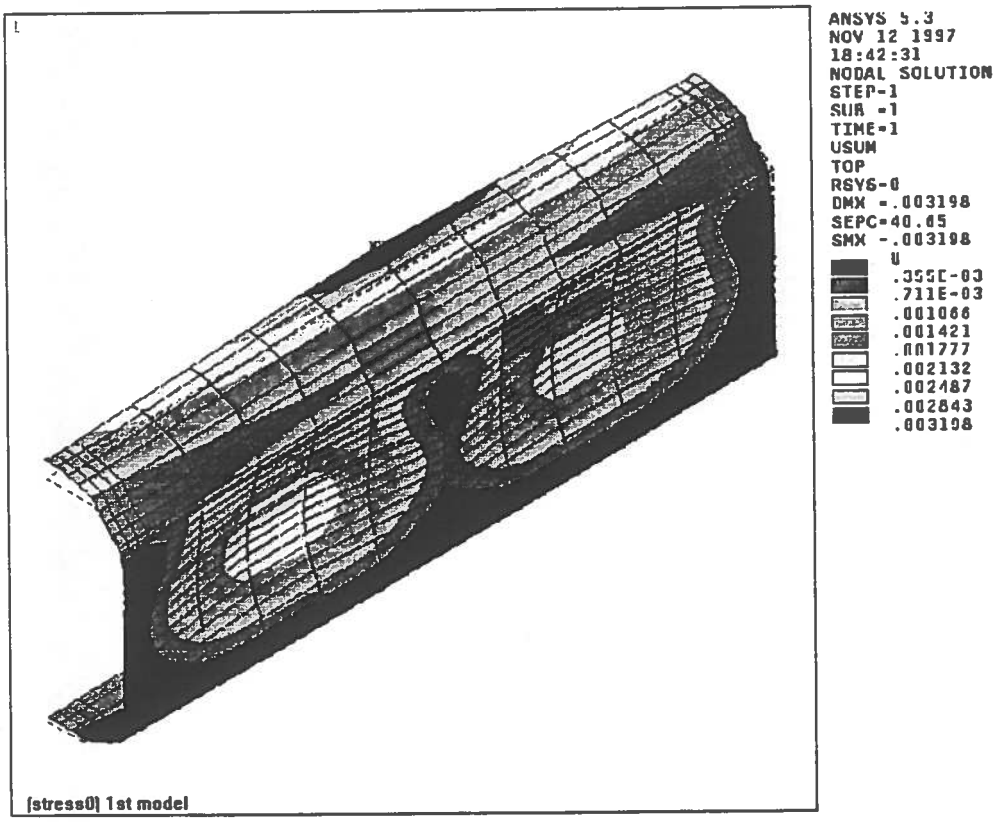

Figure 19: Total displacements (vector sum) - model without the aperture.

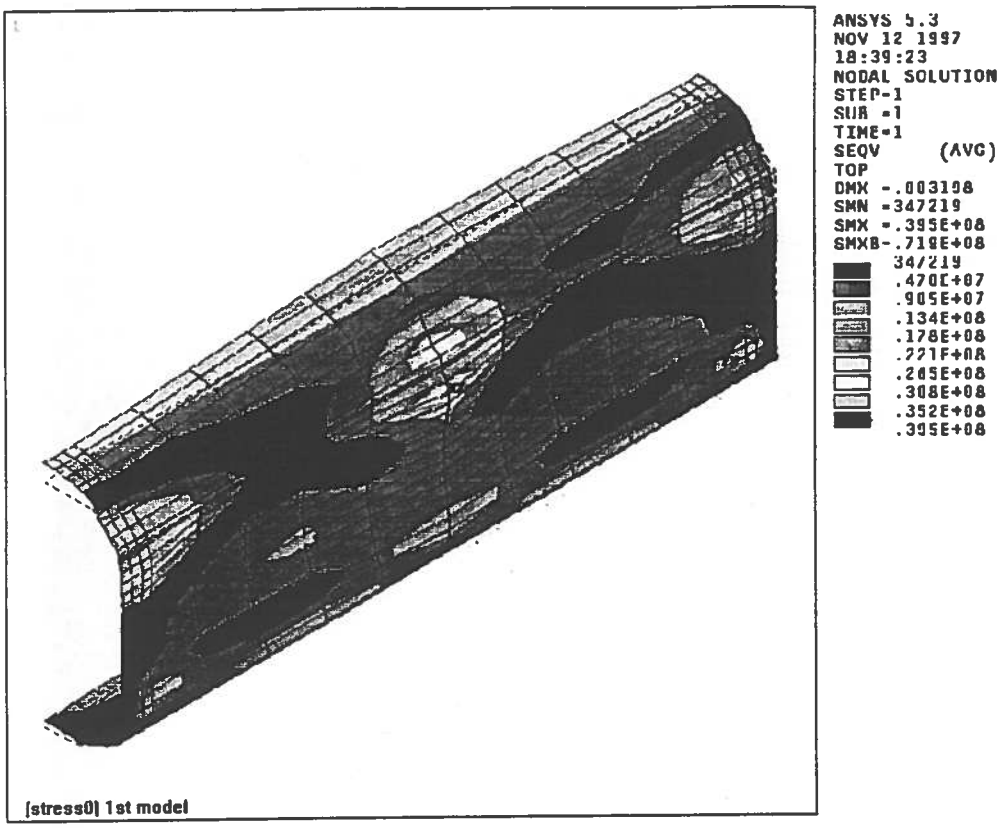

Figure 20: Equivalent stresses (Von Mises) - model without the aperture.

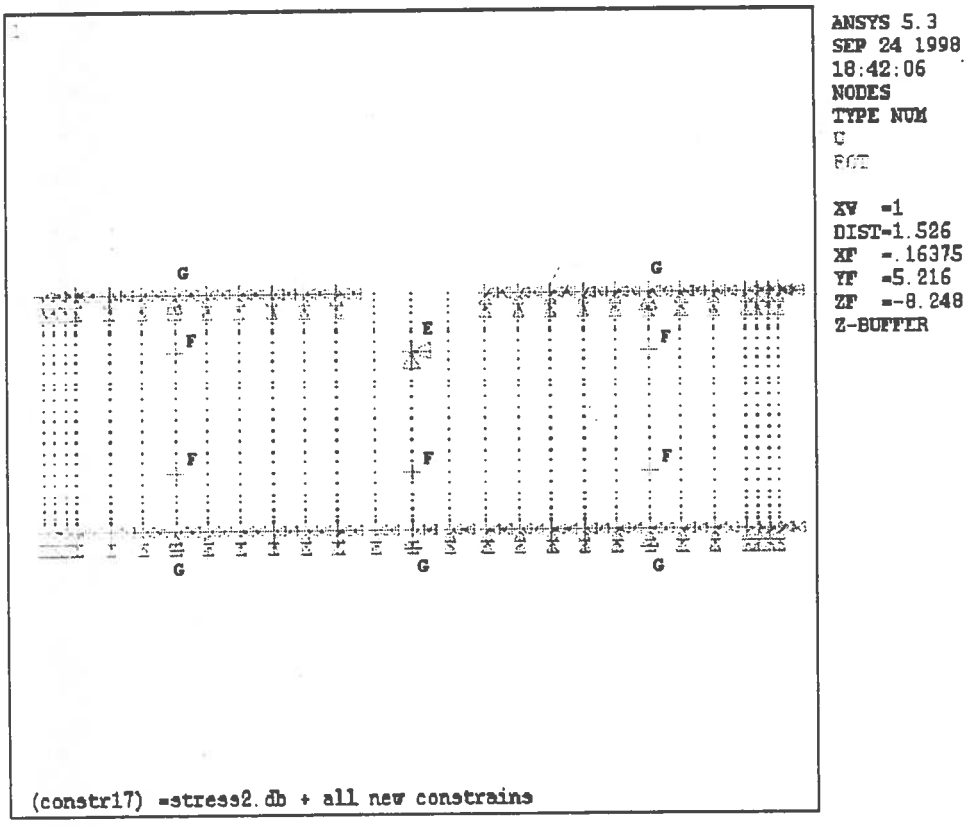

Figure 21: Constraints for stress analysis - model with the aperture.

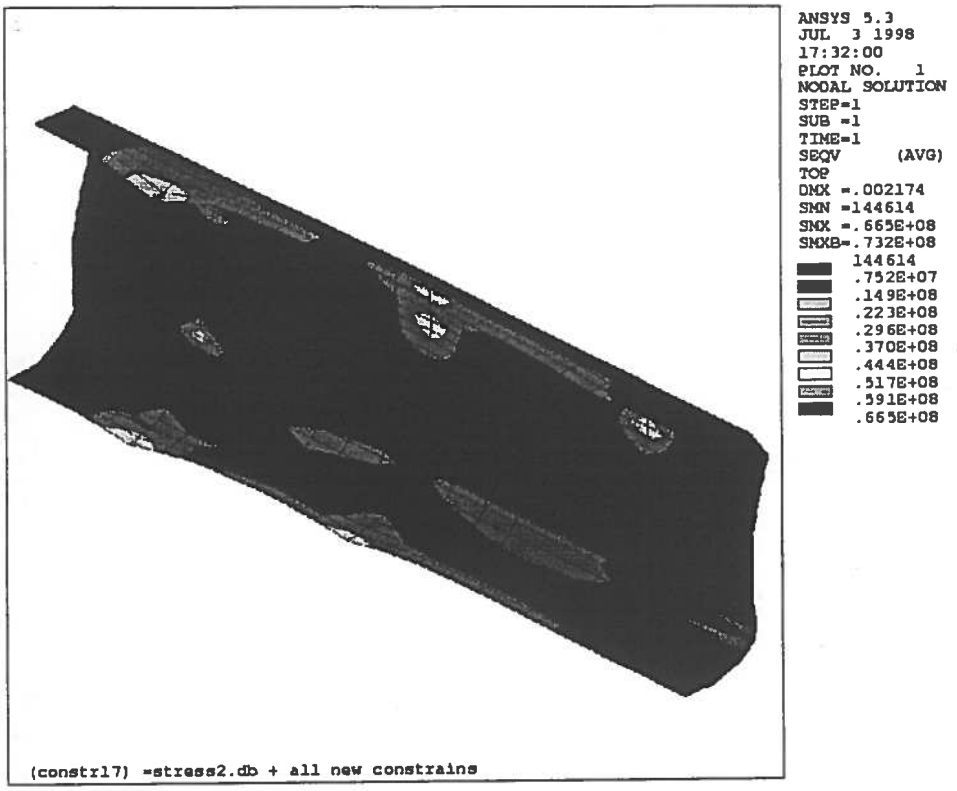

Figure 22: Total displacements (vector sum) - model with the aperture.

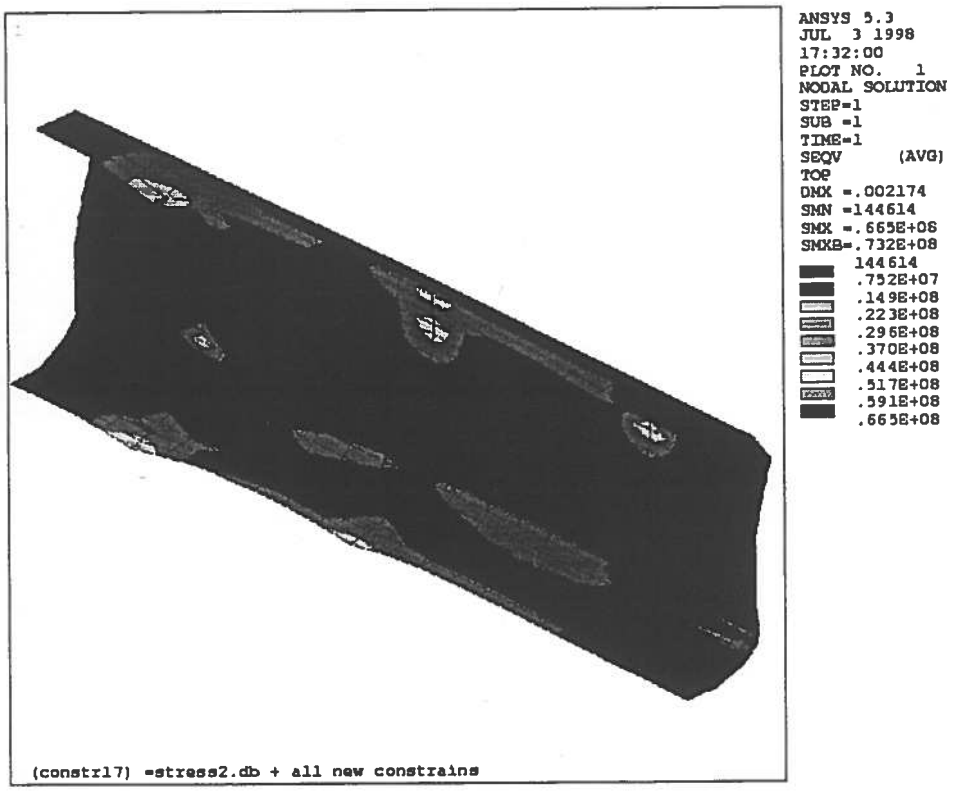

Figure 23: Equivalent stresses (Von Mises) - model with the aperture.